J Solid State Electrochem (2002) 6: 126–133
DOI 10.1007/s100080100201

ORIGINAL PAPER

H. Razmi-Nerbin · M.H. Pournaghi-Azar

Nickel pentacyanonitrosylferrate film modified aluminum electrode for electrocatalytic oxidation of hydrazine

Received: 24 August 2000 / Accepted: 5 February 2001 / Published online: 3 July 2001

Abstract The electrocatalytic oxidation of hydrazine at the aluminum electrode, modified by electroless deposition of nickel pentacyanonitrosylferrate (NiPCNF) on the surface of the electrode has been studied by cyclic voltammetry, chronoamperometry and rotating disk electrode voltammetry and the kinetics of the catalytic reaction were investigated. The results were explained using the theory of electrocatalytic reactions at chemically modified electrodes. It was found that a one-electron charge-transfer process is rate limiting and that the average values of the rate constant for the catalytic reaction and the diffusion coefficient, evaluated by different approaches, are 5.2×10^3 $M^{-1}s^{-1}$ and 8.5×10^{-6} cm^2s^{-1}, respectively. Further examinations of the modified electrodes show that the modifying layers (NiPCNF) on the aluminum substrate have reproducible behavior and a high level of stability, after exposing them in air and hydrazine solutions for a long time.

Keywords Electrocatalytic oxidation · Aluminum electrode · Modified electrode · Nickel pentacyanonitrosylferrate · Hydrazine

Introduction

Electrooxidation of hydrazine is the basis of an established fuel cell and hence is a reaction of practical importance owing to its high capacity and no contamination [1]. The mechanism and kinetics of hydrazine oxidation have been studied at several electrodes, including silver [2], nickel [3], gold [2] mercury [2, 4, 5] and platinum [5, 6, 7, 8]. Because of the large overpotential of hydrazine at conventional electrodes, it is not suited for oxidation via these electrodes. One promising approach for minimizing overvoltage effects is through the use of an electrocatalytic process at chemically modified electrodes.

One important group of inorganic compounds utilized for electrode modification and used for electrocatalytic purposes is the transition-metal hexacyanoferrates. The modification of the electrode surface by these compounds is possible in different ways:

1. By electrodeposition of the transition metal on the matrix and then electrochemical anodizing of the resulting surface in the presence of hexacyanoferrate [9, 10].
2. By immersing the electrode surface in a solution containing cyanoferrate and transition-metal ions and cycling the electrode, over a range of potentials [11, 12].
3. By electrodeposition of the transition metal on the matrix and then chemical derivatization of resulting electrode in the presence of cyanoferrate ion [13, 14].
4. By immersing the transition-metal electrode surface in a solution containing cyanoferrate ion and potentiostating the electrode at a convenient value [15].
5. By electroless deposition of the transition metal on the matrix and then chemical derivatization of the resulting surface in the presence of cyanoferrate ion [16, 17].
6. By mechanically immobilizing the transition-metal cyanate, using a paraffin-impregnated graphite electrode [18, 19, 20].
7. By an electrochemically driven insertion–substitution mechanism [21, 22].

In all cases, the insoluble transition-metal cyanoferrate is formed by electrochemical or chemical oxidation of the transition metal and subsequent reaction with cyanoferrate ion. In most of these investigations, common substrates such as Pt [10], Au [11], glassy carbon (GC) [10], Ni [12] or recently Al [16, 17] were utilized as matrices for the preparation of modified electrodes.

The mediated and electrocatalytic oxidation of hydrazine at a GC modified electrode with mixed-valence

H. Razmi-Nerbin · M.H. Pournaghi-Azar (✉)
Electroanalytical Chemistry Laboratory,
Faculty of Chemistry, University of Tabriz, Tabriz, Iran
E-mail: pournaghi@ark.tabrizu.ac.ir
Fax: +98-41-340191

Prussian blue [23, 24] and its analogs ruthenium cyanide [25], nickel and cobalt hexacyanoferrate [10, 26] films was studied. Metal pentacyanonitrosylferrate films as well as metal hexacyanoferrate on the glassy carbon electrode are useful electron-transfer mediators. There are some reports showing that the copper pentacyanonitrosylferrate film has electrocatalytic activity for the oxidation of ascorbic acid, hydrogen peroxide and for the reduction of hydrogen peroxide [27].

In order to extend the use of the aluminum matrix, which is a low-cost metal and is suitable for electroless preparation of transition-metal cyanoferrate film-modified electrodes [16], we reported recently the characteristics of a nickel pentacyanonitrosylferrate (NiPCNF) coated aluminum electrode in various solution compositions and its catalytic effect on the oxidation of ascorbic acid [17, 28]. In the present work, we describe the electrocatalytic properties of NiPCNF confined on the aluminum electrode toward the electrocatalytic oxidation of the hydrazine using various electrochemical techniques. It is also intended to determine the kinetic parameters of the catalytic oxidation of hydrazine at this electrode.

Experimental

Chemicals and reagents

An aluminum bar with purity of $99.9 \pm 0.2\%$ was used as the substrate for the electrode matrix. Nickel chloride and ammonium chloride were of analytical grade from Merck. Hydrazinium dichloride (99%) and sodium pentacyanonitrosylferrate (reagent grade) were from Merck and Riedel, respectively, and were used as received. All the solutions were prepared with distilled water.

Electrode preparation

The aluminum surface of 0.125 cm^2 fitted in a Teflon tube [16] was polished to a mirror finish, first by sandpaper (P320) and then by 0.05-μm alumina powder. The polished surface was cleaned by dipping it in concentrated HCl for about 1 min and was then rinsed with distilled water. The electroless deposition of nickel was carried out by dipping the cleaned surface of the aluminum electrode in a solution containing 0.5 M $NiCl_2$ and 1.5 M NH_4Cl of pH 1 (plating solution) for about 10–15 min. The aluminum electrode covered by metallic nickel was derivatized by immersing it in 0.5 M $NaNO_3$ and 10 mM $Na_2[Fe(CN)_5\ NO]$ solution of pH 2–3 adjusted by HNO_3 (derivatizing reagent) for about 3–4 h. In order to decrease the background current, the modified electrode was left in air for at least 1 day. This may arise from a morphological stabilization of the crystal lattice of the film or from the appearance of more Ni^{2+} cations in the crystal lattice, causing an increase in the electronic conductivity of the film. The surface concentration of the mediator in the film per unit surface area of the electrode, Γ, was determined from the area under the anodic part of the cyclic voltammograms of the NiPCNF-coated aluminum electrode. By assuming that the density of $Na_2Ni[Fe(CN)_5\ NO]$ is 1.79 gcm^{-3} [29], the thickness of the film, *d*, and the total volume concentration, c_p^0 were calculated.

Instrumentation

The electrochemical experiments were carried out using an EG&G PAR model 273 potentiostat/galvanostat coupled with an IBM personal computer connected to a Hewlett-Packard Laser Jet 5L printer. A conventional three-electrode cell was used at 25 ± 1 °C. A saturated calomel electrode, a platinum wire and the aluminum disk modified electrode were used as reference, auxiliary and working electrodes, respectively. A model 616 rotating electrode system, from EG&G PAR, was employed.

Results and discussion

Voltammetric and chronoamperometric studies

The cyclic voltammograms of the bare and NiPCNF-coated aluminum electrodes in the absence and the presence of hydrazine are shown in Fig. 1. As seen in Fig. 1, curve a, the NiPCNF-modified aluminum electrode in the blank solution (0.5 M $NaNO_3 + 0.25$ M phosphate buffer of pH 7.2) exhibits a well-behaved redox reaction at 0.55 V (curve a). Upon the addition of 2.5 mM hydrazine, an enhancement in the anodic peak current was observed and the cathodic peak current tended to disappear (curve b). This behavior is typical of that expected for mediated oxidation. It was also noteworthy that hydrazine at the bare aluminum electrode was electroinactive in this electrolytic solution (Fig. 1, curve d).

The anodic peak current observed in the presence of hydrazine increases with increasing hydrazine concentration in the solution (Fig. 2). The inset of Fig. 2 shows clearly that the plot of I_p versus hydrazine concentration between 0.0–35 mM, constituted from two linear segments with different slopes, corresponds to two different

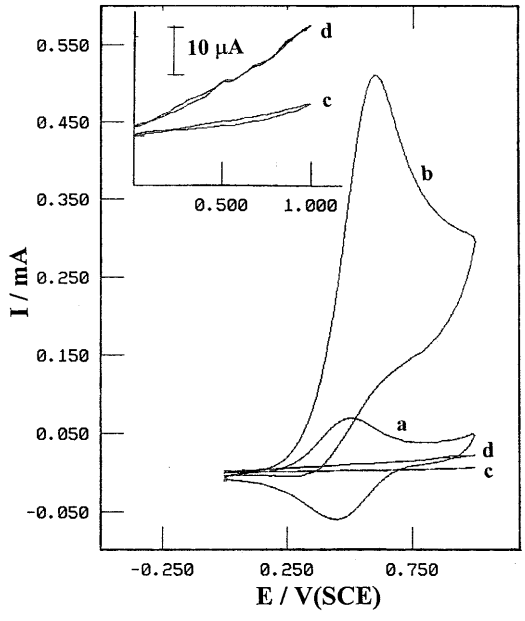

Fig. 1 Cyclic voltammograms of the nickel pentacyanonitrosylferrate (*NiPCNF*)/Al electrode (*a*, *b*) and the bare Al electrode (*c*, *d*) in the absence (*a*, *c*) and in the presence (*b*, *d*) of 2.5 mM hydrazine. *Inset*: curves *c*, *d* from the main panel with a microampere scale. Supporting electrolyte: 0.5 M $NaNO_3$ + 0.25 M phosphate buffer (pH 7.2), potential scan rate: 50 mVs^{-1}

ranges of hydrazine concentration. We ascribe this to a change in the catalytic reaction conditions arising from the formation of nitrogen gas bubbles at the surface of the film as has already been reported by others [24]. Indeed at low concentrations of hydrazine, the gas formed being negligible has no effect on the diffusion of hydrazine toward the electrode surface (gas evolution unaffected zone), while at high concentrations of hydrazine, gas evolution at the electrode surface reduces to some extent the normal diffusion of the substrate (gas evolution affected zone).

The cyclic voltammograms of the NiPCNF-coated aluminum electrode at various scan rates (25–300 m Vs^{-1}) in the presence of 2.5 mM hydrazine reveal that the catalytic effect of the NiPCNF film appeared at scan rates of up to 100 mVs^{-1} owing to a considerable catalytic reaction rate (Fig. 3). It can be noted from the inset of Fig. 3 that with increasing scan rate the peak potential for the catalytic oxidation of hydrazine shifts to more positive potentials, suggesting a kinetic limitation in the reaction between the redox sites of the NiPCNF film and hydrazine. The oxidation current for hydrazine increased linearly with the square root of the scan rate (Fig. 4A), suggesting that the reaction is mass-transfer controlled. Moreover a plot of the scan rate normalized current ($I/v^{1/2}$) versus scan rate (Fig. 4B) exhibits an indicative shape typical of an electrochemical chemical (EC) catalytic process. Note that the cyclic voltammetry of the NiPCNF/Al electrode in the absence of hydrazine at scan rates between 10 and 300 mV s^{-1} showed that the peak potential did not shift and that the current function

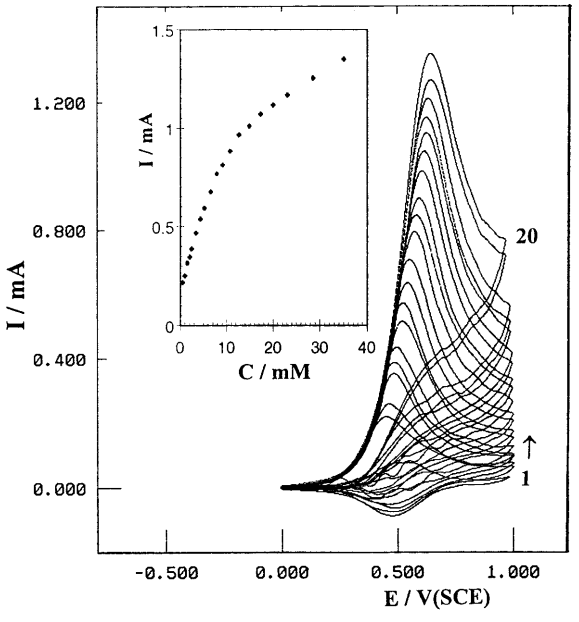

Fig. 2 Cyclic voltammograms of the NiPCNF/Al electrode in the presence of different hydrazine concentrations: (*1–20*) 0, 0.5, 1, 1.5, 2, 2.4, 3.4, 4.3, 5.2, 6.5, 7.8, 9.1, 10.7, 12.7, 14.9, 17.4, 20, 23.1, 28.6 and 35 mM, respectively. Potential scan rates: 50 mVs^{-1}; supporting electrolyte as in Fig. 1. *Inset*: variations of the anodic peak currents versus hydrazine concentrations

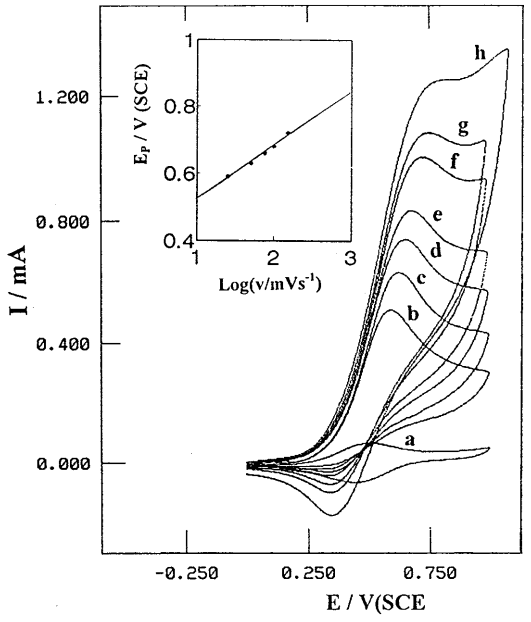

Fig. 3 Cyclic voltammograms of the NiPCNF/Al electrode in the absence (*a*) and in the presence (*b–h*) of 2.5 mM hydrazine at various potential scan rates: 25, 50, 75, 100, 150, 200 and 300 mVs^{-1}, respectively. *Insets*: variation of the anodic peak potential, E_p, versus log*v*. Supporting electrolyte as in Fig. 1

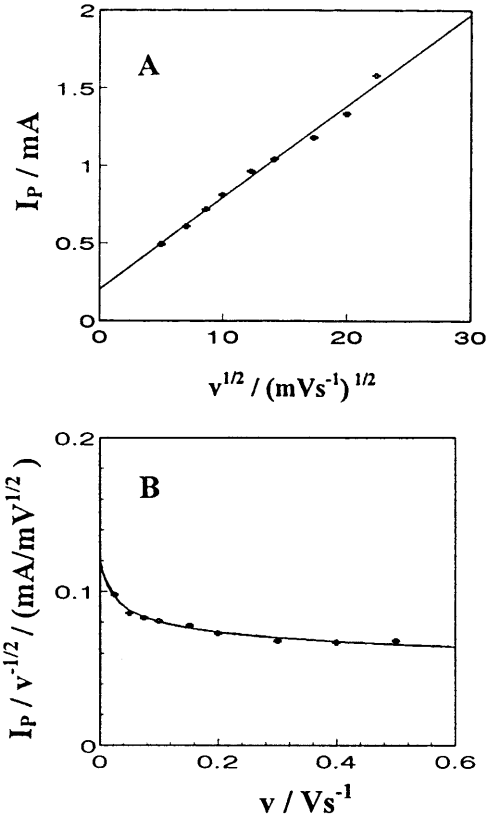

Fig. 4 Variation of **A** anodic peak currents, I_p, versus $v^{1/2}$ and **B** anodic current function $I_p/v^{1/2}$ versus $v^{1/2}$ for the cyclic voltammograms of Fig. 3

always remained constant with scan rate [17]. These confirm the absence of an ohmic drop effect on the shape of the cyclic voltammograms.

In order to obtain information on the rate-determining step, Tafel plots were drawn using the data from the rising part of the current–voltage curves at a scan rate of 10 mV s^{-1} for three different concentrations of hydrazine (Fig. 5) and a mean slope, b, of 0.184 V decade^{-1} or 5.4 (V decade^{-1})$^{-1}$ was obtained, indicating a one-electron process which was rate limiting, assuming a transfer coefficient of $\alpha = 0.68$. Note that for most of the electrode processes α ranges from 0.7 to 0.3 [30].

These results obtained from cyclic voltammetry lead to the conclusion that the overall electrochemical oxidation of hydrazine under these conditions might be controlled by the diffusion of hydrazine in the solution and a cross-exchange process between hydrazine and redox sites of the NiPCNF film. Under solution conditions (pH 7.2), where hydrazine is present in its protonated form (pK_a of hydrazine is 7.9), the process according to an EC catalytic mechanism can be expressed as

$$\mathrm{Na\,Ni\,[Fe^{II}(CN)_5NO]} \rightarrow \mathrm{Ni[Fe^{III}(CN)_5NO] + Na^+ + e^-} \quad \text{(E)}$$

$$\mathrm{Ni[Fe^{III}(CN)_5NO] + Na^+ + N_2H_5^+ \xrightarrow{k} Na\,Ni[Fe^{II}(CN)_5NO] + N_2H_3 + 2H^+} \quad \text{(C) slow}$$

$$\mathrm{3\,Ni[Fe^{III}(CN)_5NO] + 3Na^+ + N_2H_3 \rightarrow 3Na\,Ni[Fe^{II}(CN)_5NO] + N_2 + 3H^+} \quad \text{Fast}$$

The overall chemical reaction is shown as follows:

$$4\mathrm{Ni[Fe^{III}(CN)_5NO]} + 4\mathrm{Na^+} + \mathrm{N_2H_5^+} \rightarrow 4\mathrm{NaNi[Fe^{II}(CN)_5NO]} + \mathrm{N_2} + 5\mathrm{H^+}.$$

In order to obtain information on the number of electrons in the overall reaction, coulometry at a constant potential on the plate aluminum modified electrode (approximately 2 cm^2) was used and the number of electrons was found to be 4.2.

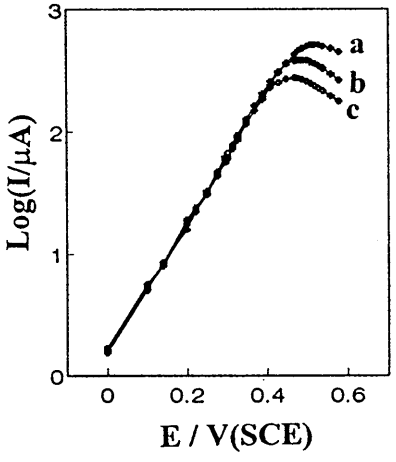

Fig. 5 Tafel plots derived from current–potential curves obtained on the the NiPCNF/Al electrode in the presence of three different hydrazine concentrations: (*a*) 1, (*b*) 2 and (*c*) 3.5 mM, at a scan rate of 10 mVs^{-1}. Supporting electrolyte as in Fig. 1

Chronoamperometry as well as the other electrochemical methods may be used for the investigation of electrode processes at chemically modified electrodes [31]. Well-defined chronoamperomgrams for the NiPCNF-film-modified aluminum electrode with a surface coverage of 6×10^{-8} mol cm^{-2} in the absence and the presence of hydrazine at applied potential steps of 0.80 and 0.00 V for forward and backward chronoamperometry, respectively, are shown in Fig. 6. Inset of Fig. 6 shows the plots of currents sampled at fixed time as a function of hydrazine concentrations. Comparison of plots 1–6 in this inset suggests that for $t < 10$ s (plots 4–6) there are two linear regions with different slopes owing to the effect of nitrogen gas bubble formation at the surface of the electrode for high concentration of hydrazine as mentioned in the cyclic voltammetric measurements, whereas for $t > 10$ s (plots 1–3), it seems that the effect of nitrogen gas bubbles was removed and only one linear region was obtained for the full hydrazine concentration range examined, but the slope decreased with the increase of the time elapsed after the potential step application.

The forward and backward potential step chronoamperometry of the modified electrode in the blank buffered solution showed very symmetrical chronoamperograms with an equal charge consumed for the oxidation and reduction of surface-confined NiPCNF sites. However, in the presence of hydrazine the charge value associated with the forward chronoamperometry, Q_f, (potential step 1: 800 mV) is significantly greater than that observed for the backward chronoamperometry, Q_b, (potential step 2: 0.0 mV). This behavior is typical of that expected for mediated oxidation.

The electrocatalytic activity of the NiPCNF-film-modified aluminum electrode toward oxidation of hydrazine was also investigated by the rotating disk electrode (RDE) voltammetry technique. The steady-state *I–E* curves were recorded for the oxidation of hydrazine at a NiPCNF-film-modified rotating aluminum disk electrode under various experimental conditions. A typical example of the *I–E* curves (RDE voltammograms) is shown in Fig. 7 for a 1.25 mM solution of hydrazine and a surface coverage of 3×10^{-8} mol cm^2.

In the case that the oxidation of hydrazine at the surface-modified aluminum electrode is controlled solely by the mass-transfer process in the solution, the relationship between the limiting current and the rotation speed should obey the Levich equation [32]:

$$I_l = I_{Lev} = 0.620nFAD^{2/3}v^{-1/6}\omega^{1/2}c_0\,, \quad (1)$$

where D, v, ω and c_0 are the diffusion coefficient, the kinematic viscosity, the rotation speed and the bulk concentration of the reactant in the solution respectively, and all other parameters have their conventional meanings. On the basis of Eq. (1), the plot of the limiting current, I_l. as a function of $\omega^{1/2}$ should be a straight line.

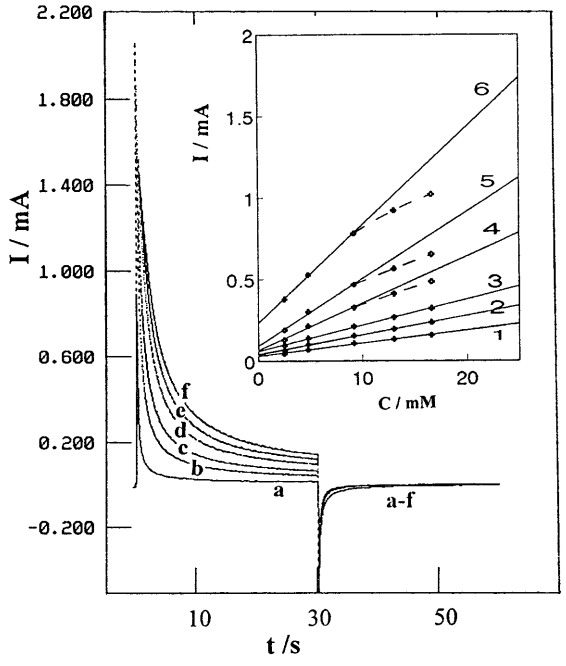

Fig. 6 Chronoamperograms obtained at the NiPCNF/Al electrode in the absence (*a*) and in the presence (*b–f*) of various concentration of hydrazine: 1, 2, 3.3, 4, 6 and 5.7 mM respectively; the first and second potential steps were 0.8 and 0.0 V, respectively. *Inset*: plots of fixed-time currents versus hydrazine concentrations (*1–6*): 25, 15, 10, 6, 4 and 2 s (times elapsed after first potential step application), respectively, derived from the data of the main panel. Supporting electrolyte as in Fig. 1

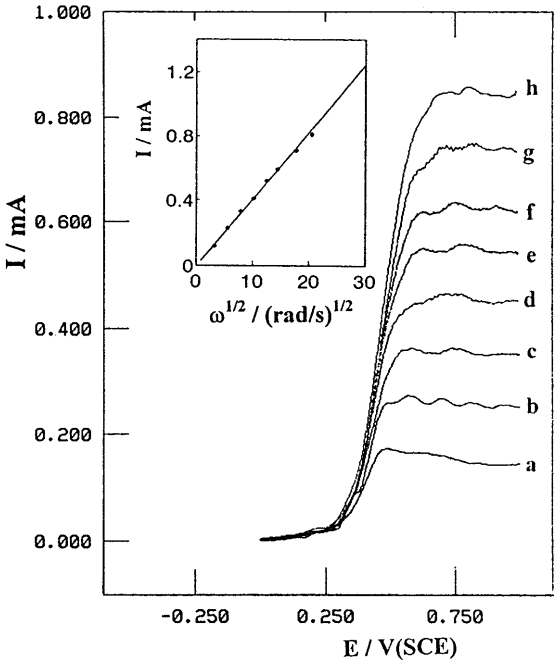

Fig. 7 Rotating disk voltammograms for 1.25 mM hydrazine oxidation at a NiPCNF/Al electrode with different rotation speeds (*a–h*): 100, 300, 600, 1000, 1500, 2000, 3000 and 4000 rpm, respectively. *Inset*: Levich plot. Supporting electrolyte as in Fig. 1; potential sweep rate 10 mVs^{-1}, $\Gamma = 3\times10^{-8}$ mol cm^{-2}

For the NiPCNF|Al modified electrode this is true for a surface coverage of 3×10^{-8} mol cm^{-2} and a hydrazine concentration lower than 1.25 mM. (Fig. 7 inset).

For a hydrazine concentration higher than 1.25 mM (i.e. 7 mM), according to the Levich plots shown in Fig. 8, the current increases with increasing electrode rotation speed, but was found to be nonlinear, including kinetic limitations (Fig. 8 inset). In this case the catalytic current, I_{cat}, corresponding to the mediated reaction is a function of Levich current, I_{Lev}, representing the mass transfer of hydrazine in the solution and the kinetic current, I_k.

Determination of diffusion coefficient of hydrazine in the solution

Chronoamperometry was used for the estimation of the diffusion coefficient of hydrazine in the solution. For an electroactive material with diffusion coefficient D, the current corresponding to the electrochemical reaction (under diffusion control) is described by Cottrell's law [33]:

$$I = nFAD^{1/2}c_0\pi^{-1/2}t^{-1/2}, \quad (2)$$

where D and c_0 are the diffusion coefficient and bulk concentration, respectively. The plot of I versus $t^{-1/2}$ will be linear, and from the slope, the value of D can be obtained. In the presence of hydrazine at long times ($t > 4$ s or $t^{-1/2} < 0.5$) the NaNi[$Fe^{II}(CN)_5NO$] oxidation is complete and the rate of electrocatalyzed hydrazine oxidation exceeds that of hydrazine diffusion from the bulk to the film solution/interface. The plot of I versus $t^{-1/2}$ ($t^{-1/2} < 0.5$) with hydrazine concentration below 2 mM, gives a straight line (Fig. 9 inset) and the slope of such lines can be used for the estimation of the diffusion coefficient of hydrazine (D).The mean value of D was found to be 8×10^{-6} cm^2 s^{-1}. The diffusion coefficient of hydrazine in the solution can also be obtained from the slope of the Levich equation. The value of D in this medium was found to be 8.1×10^{-6} cm^2 s^{-1} for the hydrazine concentration range 1–2 mM.

Kinetic process of the electrocatalytic oxidation of hydrazine

If the electron-exchange process at the electrode substrate |NiPCNF film interface is assumed to be fast, on the basis of the experimental conditions, the rate-determining step must be one of the following processes:

1. Diffusion of substrate (hydrazine) in the solution to the electrode surface.
2. Diffusion of hydrazine through the film (NiPCNF).
3. Diffusion of the electrons within the film.
4. Electron cross-exchange between the Ni[Fe^{III} $(CN)_5$ NO)] redox sites and hydrazine.

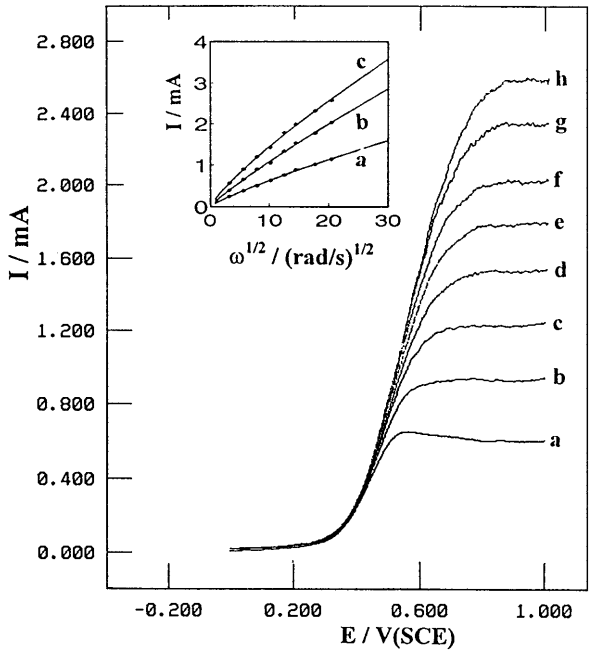

Fig. 8 Typical example of rotating disk voltammograms for hydrazine concentration higher than 1.25 mM (i.e. 7 mM) on a NiPCNF/Al electrode with different rotation speeds (*a–h*): 100, 300, 600, 1,000, 1,500, 2,000, 3,000 and 4,000 rpm, respectively. Supporting electrolyte as in Fig. 1; potential sweep rate: 10 m Vs^{-1}, $\Gamma = 3\times10^{-8}$ mol cm^{-2}. *Inset*: Levich plots for various hydrazine concentrations (*a*) 2.5, (*b*) 4.7 and (c) 7 mM

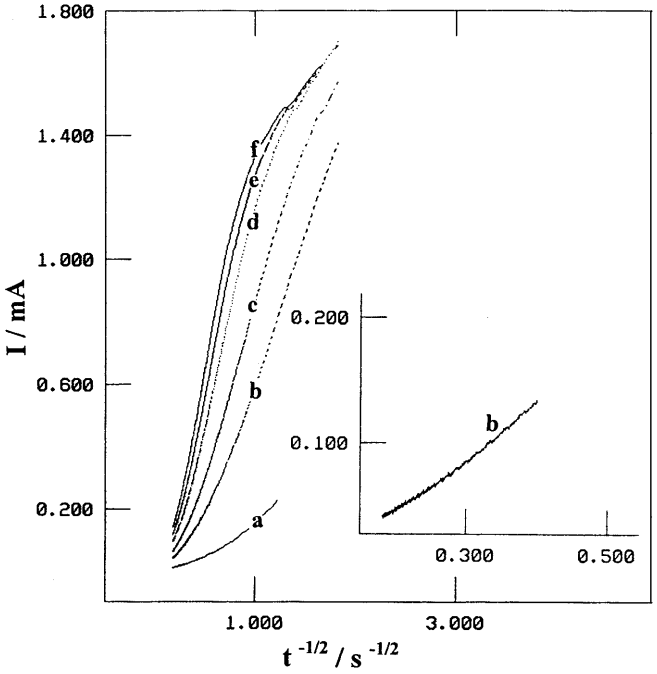

Fig. 9 Plots of I versus $t^{-1/2}$ derived from the data of chronoamperograms *b–f* of Fig. 6. *Inset*: I versus $t^{-1/2}$ (for $t^{-1/2} < 0.5$ portion of curve *b*), derived from the data of chronoamperogram (*b*) at long times, 10–30 s

A detailed description of the kinetic process of the catalytic reaction at the modified electrodes has been given by Andrieux et al.[34], leading to an expanded equation. When thin films and high substrate (hydrazine) concentrations are used, the contribution of hydrazine and electron diffusion within the NiPCNF film (like Prussian blue and its analogs) are negligibly small [24] and the mass-transport process in the solution and the catalytic reaction become dominant.

The rate-determining step is given by reaction C with a heterogeneous rate constant, k, which is representative of the catalytic reaction rate between NiPCNF on the electrode and hydrazine, diffused from the solution. The value of k can be evaluated by two different approaches.

RDE voltammetry

When the mass-transfer process in the solution and the catalytic reaction become dominant, the Koutecky–Levich equation (Eq. 3) is used for kinetic analysis.

$$\frac{1}{I_l} = \frac{1}{nFAc_0k\Gamma} + \frac{1}{0.62nFAD^{2/3}v^{-1/6}c_0\omega^{1/2}}, \qquad (3)$$

where A, c_0, k, Γ, D, v and ω are the electrode area, substrate concentration, catalytic rate constant, surface coverage, diffusion coefficient, kinematic viscosity and rotation speed. According to Eq. (3) a plot of I^{-1} versus $\omega^{-1/2}$ gives a straight line (as shown in Fig. 10A). The value of the rate constant for the catalytic reaction, k, can be obtained from the intercept of the Koutecky–Levich plot. k was found to be in the range 3.4×10^3–4.6×10^3 $M^{-1}s^{-1}$ for hydrazine concentration in the range 2.5–7 mM, using $\Gamma = 3\times10^{-8}$ molcm^{-2}. The slope of the Koutecky–Levich equation is dependent on the reactant concentration c_0. The reverse relationship between the slope of the Koutecky–Levich plots and the hydrazine concentrations (Fig. 10B) confirms that the catalytic reaction is a first-order one versus the concentration of hydrazine. The diffusion coefficient of hydrazine, D, may also be obtained from the slope of the Koutecky–Levich plots. The mean value of D was found to be 9×10^{-6} cm^2 s^{-1}, which is in good agreement with those obtained from the chronoamperometric measurements and slopes of Levich plots and values reported by others [35].

Chronoamperometry

Chronoamperometry can used for the evaluation of the catalytic rate constant. At intermediate times ($t = 250$ ms- 6 s or $t^{-1/2} = 2$–0.4, in the present work) the catalytic current (I_{cat}) is dominated by the rate of electrocatalyzed oxidation of hydrazine and the rate constant for the chemical reaction between hydrazine and redox sites of surface-confined NiPCNF is determined according to the method described in the literature [36]:

$$I_{cat}/I_L = \gamma^{1/2}[\pi^{1/2}\mathrm{erf}(\gamma^{1/2}) + \exp(-\gamma)/\gamma^{1/2}], \qquad (4)$$

where I_{cat} and I_L are the currents of the NiPCNF-modified aluminum electrode in the presence and the absence of hydrazine, respectively, and $\gamma = kc_0t$ (c_0 is the bulk concentration of hydrazine) is the argument of the error function. In the cases that γ exceeds 2, the error function is almost equal to 1 and Eq. (4) can be reduced to

$$I_{cat}/I_L = \gamma^{1/2}\pi^{1/2} = \pi^{1/2}(kc_0t)^{1/2}, \quad (5)$$

where k, c_0 and t are the catalytic rate constant, the catalyst concentration and the time elapsed. From the slope of the plot of I_{cat}/I_L versus $t^{1/2}$ we can simply calculate the value of k for a given concentration of hydrazine. One such plot, constructed from the chronoamperograms of the NiPCNF-film-modified aluminum electrode in the absence and the presence of 1 mM hydrazine is shown in Fig. 10C and value of k was found to be 5.8×10^3 $M^{-1}s^{-1}$.

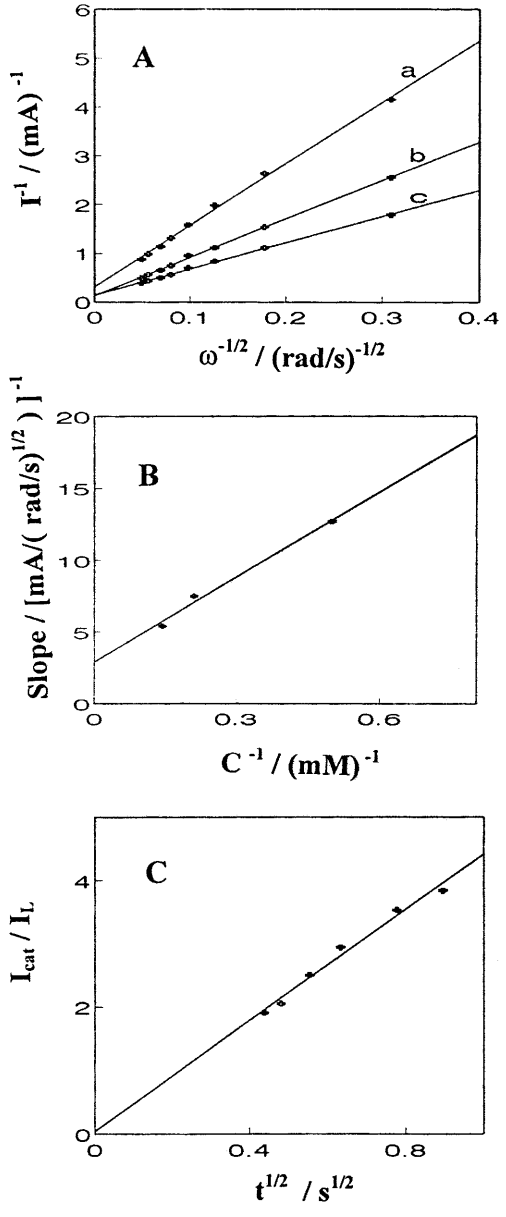

Fig. 10 **A** Koutecky-Levich plots derived from the data of the inset of Fig. 8. **B** Variation of the slope of the Koutecky–Levich plots versus the reciprocal of the hydrazine concentrations. **C** Dependence of I_{cat}/I_L on $t^{1/2}$, derived from the chronoamperogram data in the absence and the presence of 1 mM hydrazine

Stability study

The electrode exposed in air at room temperature for several months yielded good cyclic voltammogram peaks and the capacitive current decreased. Our experimental investigation indicates that NiPCNF film in the buffered electrolyte solution is stable for several manipulations The peak height and peak potential of the surface-immobilized film by cycling of the electrode potential over the range 0.0–1.3 V remains nearly unchanged (Fig. 11, curve a). The amount of degradation after 40 cycles in electrolyte solution with a scan rate of 50 mVs^{-1} was less than 2% (Fig. 11, curve b). Furthermore a negligible decrease in the height of the cyclic voltamograms was observed after construction of a ten-points calibration graph or after recording about 20 rotating disk voltammograms with a rotation speed of 50–4000 rpm. In addition the reproducibility of the electrocatalytic effect of the modified electrode was confirmed by repetitive recording of the cyclic voltammograms in hydrazine solution.

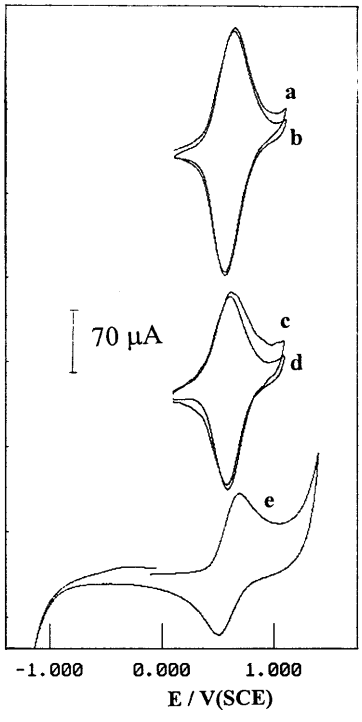

Fig. 11 Cyclic voltammograms of the NiPCNF/Al electrodes: (*a*, *c*) first cycles in supporting electrolyte, (*b*) 100th cycle, (*c*) after construction of two 20-point calibration graphs for hydrazine and (*d*) after 10 cycles over a potential range of –1.2–1.4 V. Supporting electrolyte: 0.5 M $NaNO_3$ + 0.25 M phosphate buffer (pH 7.2); potential scan rate: 50 m Vs^{-1}

Conclusion

The aluminum surface coated with NiPCNF film can catalyze the oxidation of hydrazine via surface-layer-mediated charge transfer. The charge-transfer step of the rate-limiting reaction is found to be a one-electron abstraction step; however, the final product obtained is nitrogen gas. The currents obtained in cyclic voltammetry, chronoamperometry and steady-state voltammetry are diffusion-controlled for low concentrations of hydrazine, while at higher hydrazine concentrations the slope of the currents versus the hydrazine concentration are decrease significantly, most probably because of nitrogen gas evolution The kinetic process of the catalytic reaction can be explained using chronoamperometry and RDE voltammetry. The results obtained for the rate constant and the diffusion coefficient of hydrazine in the solution, by different approaches, are in good agreement. The modified aluminum electrode prepared is stable for several months, which makes it useful for electrocatalytic oxidation of hydrazine.

References

1. Zhu Z, Ren J, Quing Z (1992) Gaoden Xuexiao Huaxue 14:1710
2. Korinek K, Korita J, Nusiloua M (1969) J Electroanal Chem 21:421
3. Felischmann M, Korinek K, Plrtcher D (1972) J Electroanal Chem 34:499
4. Eissner U, Gileadi E (1970) J Electroanal Chem 28:81
5. Harrison JA, Khan ZA (1970) J Electroanal Chem 26:1
6. Perek M, Bruckenstein S (1973) J Electroanal Chem 47:329
7. Bard AJ (1963) Anal Chem 35:1603
8. Harrison JA, Khan ZA (1970) J Electroanal Chem 28:131
9. Itaya K, Akahoshi H, Toshima S (1982) J Electrochem Soc 129:1498
10. Lin C, Bocarsly AB (1991) J Electroanal Chem 300:325
11. Cai C, Ju H, Chen H (1995) Anal Chem Acta 310:145
12. Cai C, Ju H, Chen H(1995) Anal Chem Acta 397:185
13. Gao Z, Wang G, Li P, Zhao Z (1991) Electrochim Acta 36:147
14. Arent DJ, Hidalgo-Luangdilok C, Chun JKM, Bocarsly AB (1992) J Electroanal Chem 328:295
15. Humphrey BD, Sinha S, Bocarsly AB (1987) J Phys Chem 91:586
16. Pournaghi-Azar MH, Razmi-Nerbin H (1998) J Electroanal Chem 456:83
17. Pournaghi-Azar MH, Razmi-Nerbin H (2000) Electroanalysis 12:209
18. Dostal A, Meyer B, Scholz F, Dchroder U, Bond AM, Marken F, Shaw CJ (1995) J Phys 99:2095–2103
19. Zakharchuk NF, Meyer B, Henning H, Scholz F, Jaworski A, Stojek Z (1995) J Electroanal Chem 398:23–35
20. Reddy SJ, Dostal A, Scholz F (1996) J Electroanal Chem 403:209–212
21. Dostal A, Herm M, Scholz F (1997) J Electroanal Chem 422:205
22. Kahlert H, Retter U, Lohse H, Siegler K, Scholz F(1998)J Phys Chem 102:8757–8765
23. Hou W, Wang E (1992) Anal Chim Acta 257:275
24. Scharf U, Grabner EW (1996) Electrochim Acta 41:233
25. Wang J, La Z (1989) Electroanalysis 1:517
26. Golabi SM, Noor-Mohammadi F (1998) J Solid State Electrochem 2:30
27. Gao Z, Tian ZYM, Zhao Z (1993) J Electroanal Chem 358:161
28. Pournaghi-Azar MH, Razmi-Nerbin H (2000) J Electroanal Chem 488:17
29. (1963) Hand book of chemistry and physics, 44th edn. CRC, Boca Raton, p 14
30. Bard AJ, Faulkner LR (1980) Electrochemical methods, fundamentals and applications. Wiley, New York, p 96
31. Kuo KN, Muray RW (1982) J Electroanal Chem 131:37
32. Bard AJ, Faulkner LR (1980) Electrochemical methods, fundamentals and applications. Wiley, New York, p 288
33. Bard AJ, Faulkner LR (1980) Electrochemical methods, fundamentals and applications. Wiley, New York, p 143
34. Andrieux CP, Dumas-Bouchiat JM, Saveant JM (1982) J Electroanal Chem 131:1
35. Golabi SM, Zare HR (1999) J Electroanal Chem 465:168
36. Galus Z (1976) Fundamentals of electrochemical analysis. Horwood, New York, p 313